environmental sciences proceedings

MDPI

Proceeding Paper

Impact of Rossby Waves Breaking on the Heavy Rainfall in the Selenga River Basin in July †

Olga Antokhina [1], Pavel Antokhin [1] and Gochakov Alexander [2,3,*]

[1] Laboratory of Atmosphere Composition Climatology, V.E. Zuev Institute of Atmospheric Optics of SB RAS, 663055 Tomsk, Russia; olgayumarchenko@gmail.com (O.A.); apn@iao.ru (P.A.)
[2] Siberian Regional Hydrometeorological Research Institute, Department of Information and Innovation Technologies, 630099 Novosibirsk, Russia
[3] Laboratory of Geophysical Hydrodynamics, Department of Atmosphere Dynamics, Obukhov Institute of Atmospheric Physics, Russian Academy of Sciences, Pyzhevskii per. 3, 119017 Moscow, Russia
* Correspondence: gochakov@sibnigmi.ru
† Presented at the 3rd International Electronic Conference on Atmospheric Sciences, 16–30 November 2020; Available online: https://ecas2020.sciforum.net/.

Abstract: The Selenga is one of the crucial transboundary rivers of the semi-arid Northern Eurasia belt. The Selenga basin is located in Mongolia and Russia, and it is 83.4% of the Lake Baikal basin. Atmospheric precipitation is the primary source of the river supply; most of its amount falls like rain from June to August (about 70% of the annual). In the present paper, the relationship between the heaviest rains (HR) around the Selenga River basin in July (above 90th percentile) and Rossby wave breaking (both cyclonic and anticyclonic type, AWB and CWB) was examined. The total number of HR events from 1982 to 2019 was 83. For each event, the synoptic analysis and automatic detection of breaking based on potential vorticity from 2 to 9 PVU on the 350 K were utilized. In most cases (85%) of HR, events were accompanied to the RWB. It was revealed that waves propagating along the subtropical jet were the most important. Precipitation was observed both for the period of amplitude growth and period of waves breaking (CWB or AWB). CWBs on the subtropical jet stream that occurred east to Lake Baikal were observed in most HR events.

Keywords: Selenga River; wave breaking; precipitation; heavy rain; potential vorticity

Citation: Antokhina, O.; Antokhin, P.; Alexander, G. Impact of Rossby Waves Breaking on the Heavy Rainfall in the Selenga River Basin in July. *Environ. Sci. Proc.* **2021**, *4*, 29. https://doi.org/10.3390/ecas2020-08120

Academic Editor: Anthony R. Lupo

Published: 13 November 2020

1. Introduction

The present work is a continuation of the cycle of paper aimed at clarifying the reason for low and high water in the Lake Baikal basin [1–4]. First, highlight the main points concerning this issue [1–4]. Mongolia and Transbaikalia have experienced severe drought in recent decades due to decreased precipitation and increased air temperature in the summertime [1,5–9]. A recent decade-long drought that exceeded the instrumental record [9] caused economic, social, and environmental change [10]. The drought affected the discharge of the Selenga River. The Selenga is one of the crucial transboundary rivers of the semi-arid Northern Eurasia belt. The Selenga basin is located in Mongolia and Russia, and it is 83.4% of the Lake Baikal catchment area. Atmospheric precipitation is the primary source of the river supply; most of its amount (about 450 mm per year) falls like rain from June to August (about 70% of the annual). In the last 20 years (1996–2017), the Selenga's discharge decreased significantly [1,11–13]. In the last years (2018, 2019), the water content in the Selenga basin exceeded the average [3,14]. By the end of September 2020, the Lake Baikal water level exceeded the critical point [https://www.urdupoint.com/en/world/lake-baikal-water-level-exceeds-critical-poin-1037878.html] (accessed on 1 October 2020).

Clarification of the causes of fluctuations in the Selenga runoff is essential in the face of increasing transboundary disputes and climate change [10]. In several papers [1,3–4,15–17], authors tried to find the primary driver of precipitation during midsummer in the region, including the Selenga basin. The following mechanisms of precipitation are considered: dynamic of the northern convergence area of East Asian summer monsoon, the formation of the deep midlatitudes atmospheric troughs oriented to Mongolia, stationary Rossby wave along the Asian jet, as well as atmospheric blocking in a different part of Eurasia. So, the precipitation fluctuations over the basin are, first of all, driven by the atmospheric circulation dynamics, with the role of thermodynamic factors (local convective precipitation) less important.

The recent paper by Chyi et al. 2020 [18] showed the impact of wave breaking features of blocking on the precipitation over southeastern Lake Baikal. Wave breaking accompanied by the isentropic inverse of meridional potential vorticity (PV) gradient. Such dynamical processes such as high PV-streamers and cutoff low (CL) are associated with waves breaking (overturning). As a rule, the PV-streamers and CL are associated with high precipitation (and often extreme precipitation) [19–21]. In the front part of the slow upper-level trough (associated with PV-streamer and CL), the authors observed the intense ascending motions and transport, accumulation, and the ascent of water vapor. Additionally, convective precipitation can be observed for the central part of CL because the high PV (cold air masses) leads to high vertical instability in the troposphere [21]. In [18], it was shown that both AWB and CWB blocking events have an impact on precipitation over southeastern Lake Baikal. In addition, they are characterized by a cold trough deepening from the sub-Arctic region and a ridge amplifying toward its north over central Siberia and an evident Rossby wave train over mid-latitude Eurasia.

In the present paper, the relationship between the heaviest rains (HR) around the Selenga River basin in July (above 90th percentile) and Rossby wave breaking (RWB) (both cyclonic and anticyclonic type, AWB, and CWB) was examined. The HR events have a crucial role in annual water content formation as a whole.

2. Experiments

2.1. Data

Twelve UTC atmospheric data used in this study are from the European Centre for Medium-Range Weather Forecasts ECMWF Era-Interim [22]. We used daily precipitation data from GPCC (The Global Precipitation Climatology Centre), the spatial resolution is 1° × 1° for July 1982–2016 (version GPCC Full Data Daily Version 2018, [23]) and for July 2017–2019 (version First Guess Daily Product, [24]).

2.2. Method

Precipitation: For each day of July from 1982 to 2019, the total amount of precipitation within the Selenga River basin was calculated. For entire series (1178 values), were obtained days with precipitation above or equal the 90 percentile. These days were grouped into 83 events, which we named heavy rain events (HR events).

Wave breaking: We detected waves breaking using isentropic potential vorticity (PV) [25]. RWB is characterized by a poleward intrusion of low potential vorticity (or high potential temperature) air and an equatorward intrusion of high potential vorticity (or low potential temperature) air that is dictated by the shear environment associated with the incipient Rossby wave [26]. We detected breaking for isentropic surface 350 K. We selected 350 K due to reveal the exchange along subtropical tropopause [25], which is typical for the Siberia area only in summertime. We applied synoptic analysis and automatic algorithms searching for the overturning contour from 2 to 9 PVU (with interval 0.5 PVU).

The automatic detection of RWB events in this paper is based upon the overturning contour identification technique developed by Strong and Magnusdottir, 2008 [27]. For automatically detection centers of overturning areas, we used the identification technique developed by Barnes and Hartmann, 2012 [28].

The advantages of the method for estimation of the geometry of PV contours in comparison with the calculation of the gradient of potential temperature on the dynamical tropopause (PV-Θ) are as follows:

- First of all, the PV gradient around subtropical tropopause is stronger and visible compared to the PV-Θ gradient (Figure 1).
- Second, by using the approach to define the geometry of PV, there is no need to snap to the central longitude of breaking. Therefore, we can define shifted both northward and southward breaking.

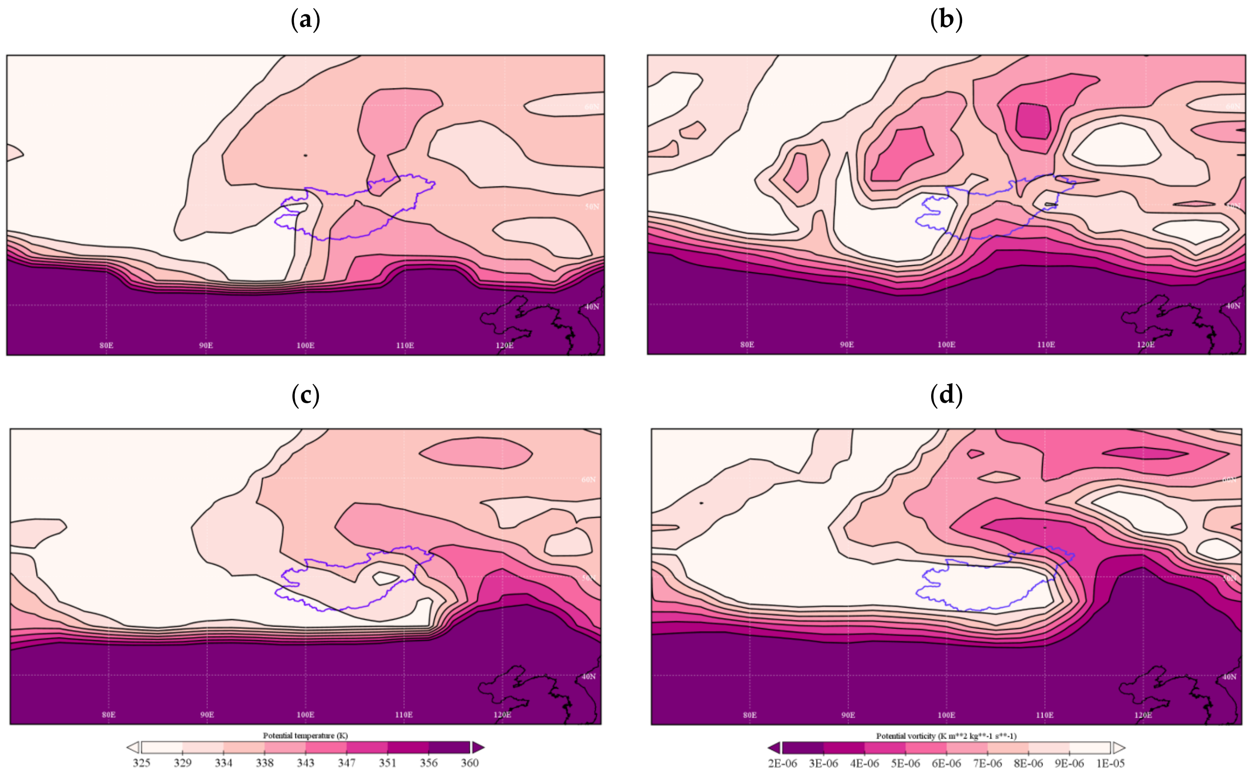

Figure 1. Wave breaking on 26–27 July 2019 based on PV-Θ (**a**,**c**) and PV on 350K (**b**,**d**). The blue contour is the Selenga basin.

3. Results

In Table 1, are shown the date of HR events, type of breaking, its duration, and center.

Table 1. Data of HR events and breaking with start and end date.

Data HR	Type of RWB	Period RWB, Center	Data HR	Type of RWB	Period RWB, Center
	90% (6 events)			**96% (10 events)**	
27.07.2011	CWB_on	26–28.07, 124° E–61° N	20.07.1987	CWB_on	19–21.07, 130° E–55° N
29.07.2005	WB	-	03-04.07.2009	AWB_I	4–5.07, 128° E–56° N
31.07.2018	WB	-	06.07.1985	WB	–
19.07.2012	AWB_I	20–21.07, 134° E–47° N	13.07.1986	CWB_on	12–13.07, 95° E–65° N
	AWB_on	16–23.07, 90° E–66° N	20–21.07.1994	CWB_I	18–21.07, 107° E–64° N
06.07.2002	AWB_I	4–8.07, 120° E–65° N	28.07.1987	CWB_I	28–30.07, 115° E–55° N
04.07.2012	CWB_on	4–5.07, 103° E–57° N	28–30.07.1982	AWB_I	28–31.07, 134° E–52° N
	91% (6 events)		21.07.1995	CWB_on	20–22.07, 102° E–73° N
24.07.1990	WB	-	27.07.2000	CWB_on	27–28.07, 130° E–61° N
20.07.2004	AWB_I	20–22.07, 128° E–55° N	28.07.1993	AWB_I	27–30.07, 120° E–60° N
23.07.1992	CWB_on	18–24.08; 124° E–60° N		**97% (12 events)**	
08.07.1996	WB	-	19.07.2000	CWB_I	19–21.07, 130° E–61° N
02.07.2008	WB	-	08.07.1986	CWB_on	5–8.07, 95° E–65° N
16.07.2009	CWB_on	16–17.07, 101° E–55° N	22.07.2019	CWB_on	22–23.07, 113° E–56° N
	AWB_on	15–17.07, 80° E–68° N	30.07.2003	CWB_on	15–31.07, 117° E, 60° N
	92% (8 events)		18.07.1983	CWB_on	20–21.07, 126° E–53° N
31.07.2013	CWB_on	31.07–1.08, 120° E–55° N	28.07.1996	CWB_I	29.07, 120E–52° N
11–13.07.2002	CWB_I	11–13.07, 135° E–52° N		AWB_on	26–28.07, 81° E–63° N
27–28.07.1997	WB	-	25–26.07.1988	CWB_on	26–18.07, 114° E–61° N
31.07.2007	CWB_on	30–31.07, 91° E–62° N	21–23.07.1993	CWB_on	20–24.07, 86° E–60° N
30.07.2012	WB	-	12.07.2015	CWB_on	11–13.07, 101° E–64° N
17.07.1989	CWB_I	17–18.07, 124° E–54° N	05–06.07.1991	CWB_on	5–7.07, 94° E–62° N
	AWB_on	14–16.07, 114° E–61° N	26–27.07.1991	AWB_on	26–28.07, 105° E–61° N
05.07.1989	CWB_on	6–8.07, 121° E–64° N		CWB_out	26.07, 110° E–52° N
	AWB_on	1–8.07, 114° E–61° N	25–26.07.1998	CWB_on	24–26.07, 119° E–56° N
12.07.1982	AWB_on	11–13.07, 91° E–69° N		**98% (9 events)**	
	CWB_out	12–15.07, 147° E–58° N	06–08.07.2006	CWB_on	6–9.07, 96° E, 64° N
	93% (4 events)		09.07.2016	AWB_I	9–10.07, 124° E–47° N
12.07.1983	AWB_on	12.07, 108° E–71° N	14–18.07.1998	CWB_on	14–17.07, 119° E–56° N
	CWB_out	13–17.07, 126° E–53° N	14.07.2010	CWB_on	13–14.07, 93° E–65° N
01.07.2018	WB	-	19.07.1984	CWB_on	17–22.07, 105° E–65° N
23.07.1983	WB	-	08–09.07.1994	CWB_on	7–10.07, 107° E–64° N
29.07.1990	CWB_on	28–29.07, 115° E–52° N	15–16.07.1990	CWB_on	12–15.07, 118° E–54° N
	94% (8 events)		06.07.2014	CWB_I	6–8.07, 124° E-57° N
20–21.07.2003	CWB_on	15–31.07, 117° E, 60° N	17–20.07.1997	CWB_on	16–18.07, 124° E–65° N
09–10.07.2008	CWB_on	9–13.07, 127° E–70° N		**99% (12 events)**	
16.07.2012	AWB_on	16–22.07, 90° E–55° N	22.07.1985	CWB_on	20–23.07, 107° E–55° N
	AWB_I	16.07, 134° E–46° N	29.07.1984	CWB_on	28–30.07, 105° E–65° N
10–11.07.2018	CWB_I	10–14.07, 145° E–65° N	21–22.07.2016	CWB_I	22–25.07, 140° E–60° N
26–28.07.1999	AWB_on	26–28.07, 85° E–70° N		AWB_on	20–21.07, 83° E–70° N
	CWB_I	28–29.07, 115° E–55° N	27–28.07.2019	CWB_on	26–29.07, 113° E–56° N
22.07.2006	AWB_on	19–22.07, 89° E–68° N	2.07.1997	CWB_on	1–3.07, 124° E–65° N
	CWB_on	21–22.07, 105° N–52° N	1.07.1999	CWB_on	3.06–2.07, 115° E–63° N
17.07.2018	WB		6–7.07.2001	CWB_on	6–10.07, 114° E–60° N
12.07.1990	CWB_on	12–15.07, 118° E–54° N	27–28.07.1983	CWB_on	27–29.07, 115° E–55° N
	AWB_on	7–11.07, 72° E–68° N	15–17.07.1991	CWB_on	15–17.07, 96° E–62° N
	95% (8 events)		6–7.07.2000	CWB_on	6–8.07, 110° E–60° N
14–15.07.1993	CWB_on	14–16.07, 127° E–50° N		AWB_on	4–5.07, 85° E–59° N
09.07.1995	AWB_I	9–11.07, 135° E–54° N	26.07.2008	AWB_I	26–27.07, 135° E–50° N
22.07.1986	CWB_I	20–22.07, 95° E–65° N	20.07.2018	AWB_I	20–23.07, 150° E–48° N
04.07.1994	CWB_on	2–5.07, 107° E–64° N			
26.07.2003	CWB_on	15–31.07, 117° E–60° N			
05–06.07.2011	CWB_on	5–6.07, 124° E–61° N			
13.07.2007	AWB_I	15–18.07, 163° E–57° N			
	AWB_on	11–14.07, 83° E–63° N			
22.07.1990	WB	-			

Propagating the low and high PV-disturbances along the area of maximal concentration of 2–6 PVU contours was observed in most of the cases. We found that several main types associated with the growth of the amplitude of the PV-disturbances lead to precipitation in the Selenga basin and waves breaking:

- CWB_on (45 events)—precipitation accompanies by CWB; in the initial (CWB_I) and mature stage (CWB_on), the breaking is located on the Selenga River basin (Figures 2 and 3).
- CWB_I (11 events)—precipitation accompanies by CWB, but in the mature stage, the breaking is located eastward of the Selenga basin. The Selenga basin is located in the stage of growth wave (CWB_I).
- AWB_I (12 Events)—precipitation accompanies by AWB, but in the mature stage, the breaking is located eastward of the Selenga basin. The Selenga basin is located in the stage of growth wave (Figure 4).
- AWB_on—usually preceded by the abovementioned CWB or AWB (Figure 5) and located westward of the the Selenga basin. In 3 cases, AWB_on preceded by CWB, which took place far eastward of the Selenga basin (12.07. 1982, 1983, and 26.07.1991). Usually, the AWB_on occurred in northern regions of Eurasia (polar jet stream), whereas the CWB_on\I and AWB_I took place in the southern region of Eurasia (subtropical jet stream).
- WB (without breaking, 12 events)—propagating of PV-disturbances did not accompany wave breaking.

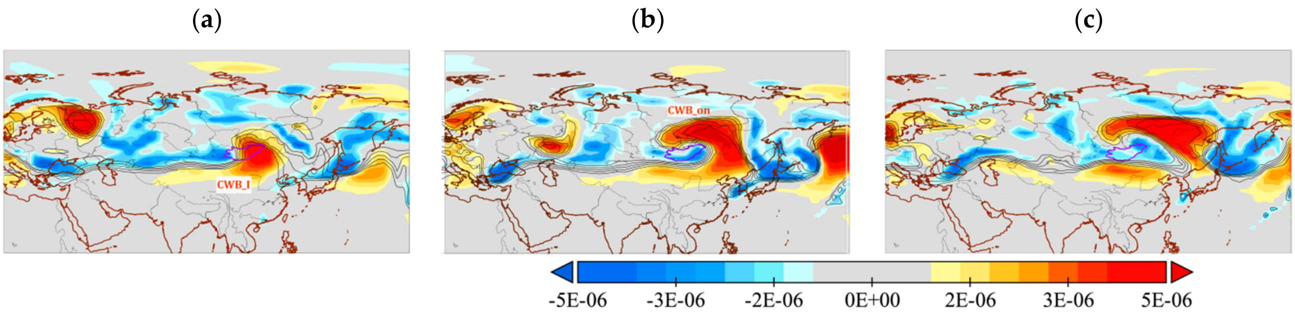

Figure 2. CWB (here and below cyclonic wave breaking) over the Selenga basin (blue contour). 6–8 July 2001. Here and below: blackline—PV counter from 2 to 9 PVU, red-blue fill—an anomaly of PV compared to the average for July 1979–2019.

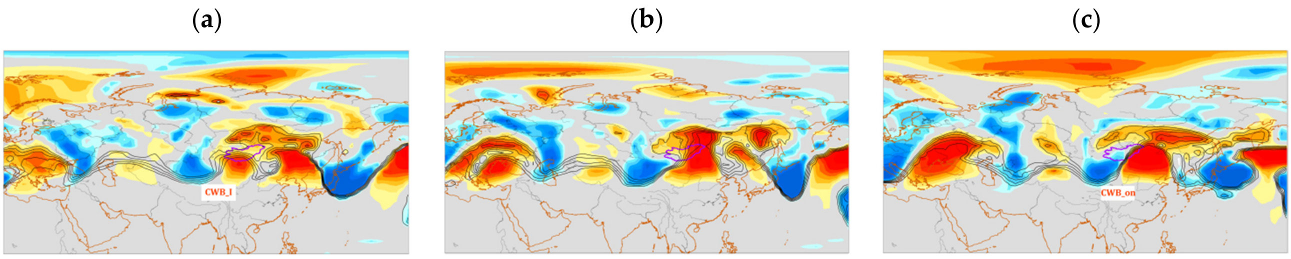

Figure 3. CWB over the Selenga basin (blue contour). 13–15 July 1998.

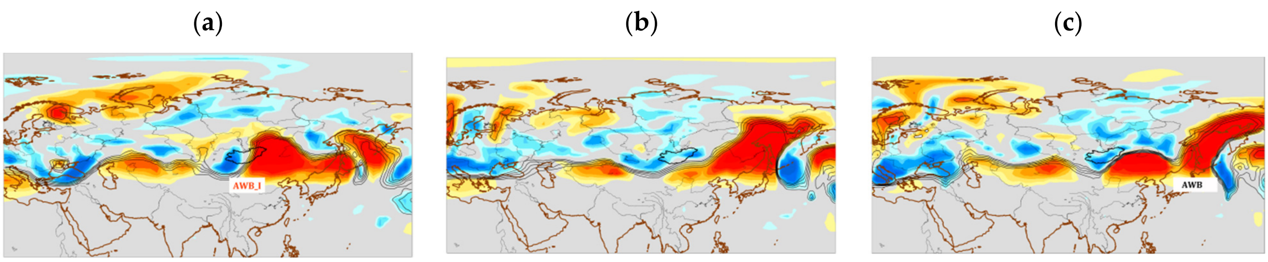

Figure 4. AWB (here and belowanticyclonic wave breaking) over the Selenga basin (blue contour). 20, 22, 24 July 2018.

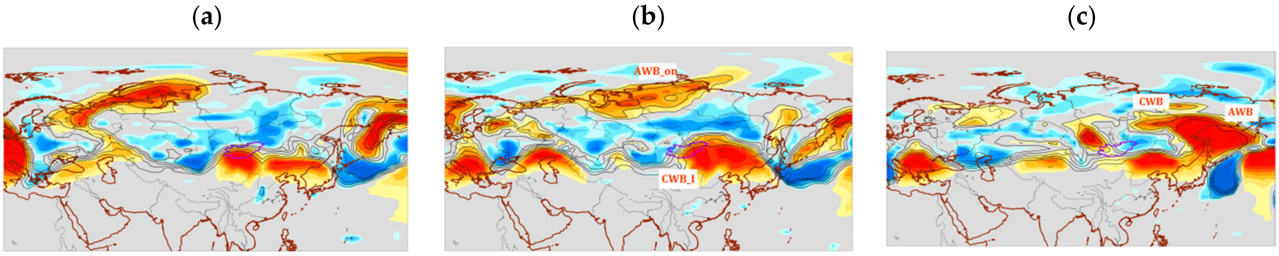

Figure 5. CWB_I and AWB_on over the Selenga basin (blue contour). 20–21, 24 July 2016.

4. Discussion

The general scheme for precipitation in the Selenga basin and breaking looked the following way:

1. Propagating the low and high PV-disturbances along the area of maximal concentration of 2–6 PVU contours (Figures 2–5);
2. Sometimes, the structure of the low and high PV-disturbances looked like a wave train (Figure 3), but it was not regular;
3. Growth of the amplitude of the PV-disturbances lead to precipitation and waves breaking;
4. Breaking can have both AWB and CWB features; for example, it can be seen in Figure 5c, where eastward, the Selenga basin breaking (overturning) simultaneously signifies both cyclonic and anticyclonic overturning. The discovered type of breaking can prove that one type of air mass simultaneously forms both the cyclone processes from the west and anticyclone from the east.

A crucial role for extreme precipitation in the Selenga River has properties of wave propagation along the subtropical jet, determining the number of circulation processes, including the polar and subtropical jet stream interaction.

In future research, we will plane to reveal the feature of water vapor transport and vertical instability for discovered cases. Additionally, it is needed for the general scheme, which unites the outcome of this paper and earlier obtained in [3,4,29].

5. Conclusions

The Selenga is one of the crucial transboundary rivers of the semi-arid Northern Eurasia belt. The Selenga basin is located in Mongolia and Russia, and it is 83.4% of the Lake Baikal basin. Atmospheric precipitation is the primary source of the river supply; most of its amount falls like rain from June to August (about 70% of the annual). In the present paper, the relationship between the heaviest rains (HR) around the Selenga River basin in July (above 90th percentile) and Rossby wave breaking (both cyclonic and anticyclonic type, AWB and CWB) was examined. Atmospheric data used in this study are from the European Centre for Medium-Range Weather Forecasts ECMWF Era-Interim; precipitation data—from GPCC (The Global Precipitation Climatology Centre).

The total number of HR events from 1982 to 2019 was 83. We detected waves breaking using isentropic potential vorticity (PV). For each event, the synoptic analysis and automatic detection of breaking based on potential vorticity from 2 to 9 PVU on the 350 K were utilized. In most cases (85%) of HR, events were accompanied to the RWB. It was revealed that waves are propagating along the subtropical jet were the most important. Precipitation was observed both for the period of amplitude growth and period of waves breaking (CWB or AWB). CWBs on the subtropical jet stream that occurred east to Lake Baikal were observed in most HR events.

Supplementary Materials: The following are available online at https://www.mdpi.com/article/10.3390/ecas2020-08120/s1, Video S1: the height (hPa) of the dynamical tropopause (2PVU) for CWB on 27 July 2019.

Author Contributions: Conceptualization, O.A.; methodology, O.A and G.A.; software, G.A and P.A.; validation, O.A., P.A. and G.A.; formal analysis, O.A.; investigation, O.A.; resources, P.A.; data curation, G.A. and P.A; writing—original draft preparation, O.A.; writing—review and editing, O.A.; visualization, O.A. and G.A; supervision, O.A.; project administration, O.A.; funding acquisition, G.A. All authors have read and agreed to the published version of the manuscript.

Funding: This research was funded by the Ministry of Science and Higher Education of the Russian Federation (budget funds for IAO SB RAS) (state registration number AAAA-A17-117021310142-5). Gochakov Alexander performed the automatic detection of RWB events described in the paragraph "Method" of Section 2 with the support of the Russian Science Foundation project, grant number 19-17-00248.

Acknowledgments: We want to express our gratitude to E. N. Osipchuk (Ph.D., Melentiev Energy Systems Institute, Siberian Branch, Russian Academy of Sciences) who prepared data catchment areas of Lake Baikal and River Selenga. We thank The Global Precipitation Climatology Centre (Public Datasets: http://ftp-anon.dwd.de/), especially Andreas Becker (Head Precipitation Monitoring Unit (KU42) and Global Precipitation Climatology Centre (GPCC)) and European Centre for Medium-Range Weather Forecasts (Public Datasets: https://apps.ecmwf.int/datasets/ (accessed on 1 October 2020).

Conflicts of Interest: The authors declare no conflict of interest.

References

1. Berezhnykh, T.V.; Marchenko, O.Y.; Abasov, N.V.; Mordvinov, V.I. Changes in the summertime atmospheric circulation over East Asia and formation of long-lasting low-water periods within the Selenga river basin. *Geogr. Nat. Resour.* **2012**, *33*, 223–229, doi:10.1134/s1875372812030079.
2. Sinyukovich, V.N.; Sizova, L.N.; Shimaraev, M.N.; Kurbatova, N.N. Characteristics of current changes in water inflow into Lake Baikal. *Geogr. Nat. Resour.* **2013**, *34*, 350–355, doi:10.1134/s1875372813040082.
3. Antokhina, O.Y.; Latysheva, I.V.; Mordvinov, V.I. A Cases Study Of Mongolian Cyclogenesis During The July 2018 Blocking Events. *Geogr. Environ. Sustain.* **2019**, *12*, 66–78, doi:10.24057/2071-9388-2019-14.
4. Antokhina, O.Y.; Antokhin, P.N.; Martynova, Y.V.; Mordvinov, V.I. The Linkage of the Precipitation in the Selenga River Basin to Midsummer Atmospheric Blocking. *Atmosphere* **2019**, *10*, 343, doi:10.3390/atmos10060343.
5. Davi, N.K.; Pederson, N.; Leland, C.; Nachin, B.; Suran, B.; Jacoby, G.C. Is eastern Mongolia drying? A long-term perspective of a multidecadal trend. *Water Resour. Res.* **2013**, *49*, 151–158, doi:10.1029/2012wr011834.
6. Schubert, S.D.; Wang, H.; Koster, R.D.; Suarez, M.J.; Groisman, P.Y. Northern Eurasian Heat Waves and Droughts. *J. Clim.* **2014**, *27*, 3169–3207, doi:10.1175/jcli-d-13-00360.1.
7. Obyazov, V.A. Regional response of surface air temperatures to global changes: Evidence from the Transbaikal region. *Dokl. Earth Sci.* **2015**, *461*, 375–378, doi:10.1134/s1028334x15040054.
8. Erdenebat, E.; Sato, T. Recent increase in heat wave frequency around Mongolia: Role of atmospheric forcing and possible influence of soil moisture deficit. *Atmospheric Sci. Lett.* **2016**, *17*, 135–140, doi:10.1002/asl.616.
9. Hessl, A.E.; Anchukaitis, K.J.; Jelsema, C.; Cook, B.; Byambasuren, O.; Leland, C.; Nachin, B.; Pederson, N.; Tian, H.; Hayles, L.A. Past and future drought in Mongolia. *Sci. Adv.* **2018**, *4*, e1701832, doi:10.1126/sciadv.1701832.
10. Kasimov, N.; Karthe, D.; Chalov, S. Environmental change in the Selenga River—Lake Baikal Basin. *Reg. Environ. Chang.* **2017**, *17*, 1945–1949, doi:10.1007/s10113-017-1201-x.
11. Chalov, S.R.; Jarsjö, J.; Kasimov, N.S.; Romanchenko, A.O.; Pietroń, J.; Thorslund, J.; Promakhova, E.V. Spatio-temporal variation of sediment transport in the Selenga River Basin, Mongolia and Russia. *Environ. Earth Sci.* **2015**, *73*, 663–680, doi:10.1007/s12665-014-3106-z.
12. Moreido, V.M.; Kalugin, A.S. Assessing possible changes in Selenga R. water regime in the XXI century based on a runoff formation model. *Water Resour.* **2017**, *44*, 390–398, doi:10.1134/s0097807817030149.
13. Frolova, N.L.; Belyakova, P.A.; Grigoriev, V.Y.; Sazonov, A.A.; Zotov, L.V.; Jarsjö, J. Runoff fluctuations in the Selenga River Basin. *Reg. Environ. Chang.* **2017**, *17*, 1965–1976, doi:10.1007/s10113-017-1199-0.
14. Ilicheva, E.; Pavlov, M.; Shchipanova, E.; Gavrilova, A. Relief formation of the Selenga River delta in different periods of water content during the technogenic stage of development. *E3S Web Conf.* **2020**, *163*, 05004, doi:10.1051/e3sconf/202016305004.
15. Iwasaki, H.; Nii, T. The Break in the Mongolian Rainy Season and Its Relation to the Stationary Rossby Wave along the Asian Jet. *J. Clim.* **2006**, *19*, 3394–3405, doi:10.1175/jcli3806.1.
16. Li, J.; Ruan, C. Corrigendum: The North Atlantic-Eurasian teleconnection in summer and its effects on Eurasian climates (2018 Environ. Res. Lett. 13 024007). *Environ. Res. Lett.* **2018**, *13*, 129501, doi:10.1088/1748-9326/aaeb56.
17. Iwao, K.; Takahashi, M. A Precipitation Seesaw Mode between Northeast Asia and Siberia in Summer Caused by Rossby Waves over the Eurasian Continent. *J. Clim.* **2008**, *21*, 2401–2419, doi:10.1175/2007jcli1949.1.
18. Chyi, D.; Xie, Z.; Shi, N.; Guo, P.; Wang, H. Wave-Breaking Features of Blocking over Central Siberia and Its Impacts on the Precipitation Trend over Southeastern Lake Baikal. *Adv. Atmos. Sci.* **2019**, *37*, 75–89, doi:10.1007/s00376-019-9048-3.

19. Martius, O.; Zenklusen, E.; Schwierz, C.; Davies, H.C. Episodes of alpine heavy precipitation with an overlying elongated stratospheric intrusion: A climatology. *Int. J. Clim.* **2006**, *26*, 1149–1164, doi:10.1002/joc.1295.
20. Appenzeller, C.; Davies, H.C. Structure of stratospheric intrusions into the troposphere. *Nat. Cell Biol.* **1992**, *358*, 570–572, doi:10.1038/358570a0.
21. Awan, N.K.; Formayer, H. Cutoff low systems and their relevance to large-scale extreme precipitation in the European Alps. *Theor. Appl. Clim.* **2016**, *129*, 149–158, doi:10.1007/s00704-016-1767-0.
22. Dee, D. P., Uppala, S. M., Simmons, A. J., Berrisford, P., Poli, P., Kobayashi, S.; Rosnay, P.D.; Tavolato, C.; Thépaut, J.-N.; Vitart, F.; et al. The ERA-Interim reanalysis: Configuration and performance of the data assimilation system. *Q. J. R. Meteorol. Soc.* **2011**, *137*, 553–597.
23. Ziese, M.; Rauthe-Schöch, A.; Becker, A.; Finger, P.; Meyer-Christoffer, A.; Rudolf, B.; Schneider, U. GPCC Full Data Daily Version. 2018 at 1.0°: Daily Land-Surface Precipitation from Rain-Gauges built on GTS-based and Historic Data. 2018. Available online: https://opendata.dwd.de/climate_environment/GPCC/html/gpcc_firstguess_daily_doi_download.html (accessed on 1 October 2020.).
24. Schamm, K., and Coauthors, 2013: GPCC First Guess Daily Product at 1.0°: Near Real-Time First Guess Daily Land-Surface Precipitation from Rain-Gauges based on SYNOP Data. Available online: https://opendata.dwd.de/climate_environment/GPCC/html/fulldata-daily_v2018_doi_download.html (accessed on 1 October 2020.).
25. Postel, G.A.; Hitchman, M.H. A Climatology of Rossby Wave Breaking along the Subtropical Tropopause. *J. Atmos. Sci.* **1999**, *56*, 359–373, doi:10.1175/1520-0469(1999)0562.0.co;2.
26. Thorncroft, C.D.; Hoskins, B.J.; Mcintyre, M.E. Two paradigms of baroclinic-wave life-cycle behaviour. *Q. J. R. Meteorol. Soc.* **1993**, *119*, 17–55.
27. Strong, C.; Magnusdottir, G. Tropospheric Rossby Wave Breaking and the NAO/NAM. *J. Atmos. Sci.* **2008**, *65*, 2861–2876, doi:10.1175/2008jas2632.1.
28. Barnes, E.A.; Hartmann, D.L. Detection of Rossby wave breaking and its response to shifts of the midlatitude jet with climate change. *J. Geophys. Res. Space Phys.* **2012**, *117*, 117, doi:10.1029/2012jd017469.
29. Antokhina, O.Y. Atmospheric Precipitation Within the Selenga River Basin and Large-Scale Atmospheric Circulation Over Eurasia in July. *Geogr. Nat. Resour.* **2019**, *40*, 373–383, doi:10.1134/s1875372819040097.